

Molecular Dynamics Simulations of Omega-3 and Omega-6 Lipid Mediators as Partial Agonists of PPAR γ

Simulações de Dinâmica Molecular de Mediadores Lipídicos Ômega-3 e Ômega-6 como Agonistas Parciais do PPAR γ

Fernando Freitas Siqueira Silva,^a Roberto Ribeiro Faria,^{a,b} Vinícius Schmitz Nunes,^{a,c} Odonório Abrahão Júnior^{a,*}

^a Universidade Federal do Triângulo Mineiro, Instituto de Ciências Biológicas e Naturais, Laboratório de Química Computacional Medicinal, Praça Manoel Terra 330, CEP 38015-050, Uberaba-MG, Brasil

^b Instituto Federal de Minas Gerais – IFMG, CEP 33805-488, Ribeirão das Neves-MG, Brasil

^c Universidade Federal do Rio de Janeiro, Programa de Pós-Graduação em Produtos Bioativos e Biotecnologia, CEP 27930-560, Macaé-RJ, Brasil

*E-mail: odonorio.junior@uftm.edu.br

Submissão: 25 de Setembro de 2024

Aceite: 19 de Dezembro de 2024

Publicado online: 13 de Janeiro de 2024

Peroxisome Proliferator-Activated Receptors (PPARs) are nuclear receptor proteins vital for metabolism, cell growth, cell differentiation, autoimmune diseases, and inflammation resolution. However, the activation mechanism by lipid-mediating agonists remains unclear. This study explores the molecular interactions and per-residue binding energy calculations between the PPAR γ subtype and four lipid mediators from n-3 and n-6 fatty acids: AA, DHA, 4HDHA, and 9HODE, identified as natural PPAR γ agonists. These findings reveal the intricate atomic-level interactions between particular residues and ligands, which are critical for determining agonistic activity. The most relevant residues were located in the loop, sheets, and H3 helix of the receptor. Positively charged residues such as K263, K265, R280, and R288 were prominent, with hydrophobic residues I281, L330, I341, and C285 also playing significant roles in ligand affinity. Residues R280, Y327, S342, and K367 were notable for persistent hydrogen bonds. The lipid carboxylate groups form stronger contacts through hydrogen bonds and electrostatic interactions than the hydroxyl groups of oxidized lipids. This study sheds new insights on the molecular mechanisms underlying the preferences of these lipid mediators, aiding the development of safer and more effective PPAR γ -targeted therapies inspired by the agonistic properties of its endogenous ligands.

Keywords: Molecular dynamics; PPAR γ ; PUFAs; Omega-3; Omega-6; lipid mediators.

1. Introduction

Lipid mediators (LMs) are signaling molecules derived from fatty acids that are typically exported to the extracellular space, where they bind to specific G protein-coupled receptors (GPCRs) on the cell surface.¹ However, an increasing body of research has indicated that LMs from various classes can also function as agonists of peroxisome proliferator-activated receptors (PPARs), members of the nuclear receptor (NR) superfamily.² Within this superfamily, three subtypes of PPARs have been identified: PPAR α , PPAR β/δ , and PPAR γ .³

Since, in the mid-1990s, PPAR γ was determined to be a molecular target of the insulin-sensitizing and antidiabetic agent thiazolidinediones (TZDs), several other physiological functions of the receptor, such as its role in immunomodulation and cancer, have been discovered and explored.⁴⁻⁹ However, severe adverse effects have been associated with receptor activation by highly potent ligands or full agonists such as TZDs.¹⁰⁻¹¹ Therefore, research has focused on studying and exploring natural endogenous ligands that often act as partial agonists. Although partial agonists have reduced potency or efficacy for receptor activation, leading to a more attenuated physiological response, such activation is often associated with fewer undesirable events.¹²⁻¹⁴

The PPAR γ ligand-binding pocket (LBP) is a bulky cavity that is larger than the pockets of other NRs and can accommodate many different ligands in different positions.¹⁵ Among the physiologically relevant ligands of PPARs, more hydrophobic, saturated fatty acids are preferred by PPAR α and, to a lesser extent, by PPAR β/δ , while PPAR γ prefers more hydrophilic lipids, as prostaglandins, leukotrienes, phospholipids and polyunsaturated fat acids (PUFAs), including essential fat acids from the omega-3 (n-3) and omega-6 (n-6) series.^{3,16,17} Diets rich in essential fatty acids are linked to several health benefits, including inflammatory and autoimmune diseases, and the prevention and treatment of cardiovascular diseases.¹⁸⁻²¹ Additionally, inflammatory conditions create a microenvironment that promotes enzymatic and nonenzymatic oxidation of PUFAs, to molecules such as hydroxy, oxo, and nitro-fatty acids, resulting in an increase in electrophilic fatty acids levels and providing additional intracellular ligands to PPAR γ .^{3,22} Many metabolic and inflammatory events are regulated by a population of enzymes and other redox potential-dependent proteins that are responsive to electrophilic lipid derivatives.¹⁷

Computational studies involving PPAR γ and its different natural and synthetic agonists, especially docking and molecular dynamics, have revealed specific ligand–residue interactions and binding affinity between these ligands and the receptor.^{23–29} In this study, Molecular Dynamics (MD) calculations were used to analyze the molecular interactions between PPAR γ and four endogenous LMs identified as partial receptor agonists: arachidonic acid (AA, n-6), docosahexaenoic acid (DHA, n-3), 9-hydroxyoctadecadienoic acid (9HODE, n-6), and 4-hydroxydocosahexaenoic acid (4HDHA, n-3). 4HDHA and 9HODE are hydroxylated (oxidized) metabolites derived from DHA and AA, respectively, which are stronger activators of PPAR γ than their nonoxidized counterparts. Moreover, the serum concentrations of 4HDHA and 9HODE in mammalian models were higher than those of other AGE oxidized metabolites and were consistent with the levels required for PPAR γ activation.^{15,30–32} Using these criteria, these four fatty acids were selected to compare PPAR γ interactions with oxidized and nonoxidized LMs, understand the agonistic mechanisms of these lipids at the molecular and atomic levels, and support the development of agonists inspired by the natural resolution of inflammation, while minimizing the adverse effects that persist in many current therapies targeting PPAR γ .

2. Methods

2.1. Protein model and ligands preparation

A model file for the PPAR γ ligand-binding domain (LBD) was constructed from three crystal structures (PDB ID codes: 3DZU, 3DZY, and 3E00) using Modeller version 9.20.^{33,34} The quality assessment involved the generation of 50 models and the evaluation of each model using Ramachandran plots and ERRAT.³⁵

Ligands were designed using Maestro.³⁶ Their carboxylic acid groups remained deprotonated, consistent with the pH of 7.2–7.4.

2.2. Molecular docking

Molecular docking was conducted using the DockThor program to generate protein–ligand complexes for MD simulations. The grid box was configured to center the lipid mediator within the receptor binding site, with coordinates of –8.684, 24.634, and 14.025 for the x, y, and z axes, respectively. A discretization value of 0.2755 was assigned, resulting in 942,400 grid points. Default parameters were used for the genetic algorithm in DockThor.^{37,38}

2.3. Molecular dynamics simulations

MD simulations were employed to investigate the dynamic behavior, conformational changes, and molecular

interactions of PPAR γ with ligands. Input preparation for all the complexes and apo-protein systems was performed using the CHARMM-GUI tool.³⁹ The ligands were parameterized using CGenFF.^{40,41} The complexes were constructed based on the ligand docking poses with the lowest total energy (Table S1, Supplementary Material). The water box dimensions were set at 100 Å × 80 Å × 60 Å with a 12 Å spacing between the protein and the boundary. K⁺ and Cl[–] ions were added at a concentration of 0.15 M for system neutrality. The CHARMM36 force field was employed to model protein–ligand interactions.⁴²

The MD protocol included energy minimization using the steepest descent method with 10,000 steps to remove local atomic collisions, conducted in two stages, with and without restrictions on the protein and ligand atoms. The temperature was gradually increased from 50 to 310 K in the NVT ensemble over 500 ps of MD simulations with the restrained nonhydrogen atoms. Equilibration was achieved through 10 ns of NPT ensemble simulations at 310 K and 1 bar with a 1 fs time step. Production MD simulations were conducted in an NPT ensemble using the leapfrog algorithm with a 2 fs time step, recording conformations every 10 ps. The temperature was maintained at 310 K using a Nose-Hoover thermostat with a relaxation time of 0.1 ps, while the pressure was maintained at 1.0 bar using a Parrinello–Rahman barostat with a relaxation time of 10 ps and a compressibility of 4.5×10^{-6} (kJ.mol⁻¹.nm⁻³)⁻¹.^{43,44} The Lincs algorithm was used to constrain all-bond stretching and bending motions. Short-range electrostatic and van der Waals interactions utilized a 1.1 nm cutoff, while long-range electrostatic contributions were determined using the particle mesh Ewald (PME) method.⁴⁵ GROMACS-2019.6 was employed for all simulations, with triplicate production runs for complex systems and a single 500 ns simulation for the apo form of PPAR γ .⁴⁶

To assess which residues were engaged in hydrogen bonding, the VMD Timeline Hydrogen Bonds was used to calculate the hydrogen bond frequencies during the simulations for each replica separately, using a donor–acceptor distance cut-off of 3.5 Å and a hydrogen-donor–acceptor angle cut-off of 30°. An additional calculation employing different distance and angle cut-offs was carried out for comparison using AMBER tool.⁴⁸ Results analysis was focused on interactions that occurred with a frequency $\geq 10\%$ (normalized to 0.1) in at least one of the replicas.

2.4. Molecular mechanics Poisson–Boltzmann surface area

To calculate the binding affinity, frames were collected at 0.2 ns intervals from 300 and 500 ns trajectories, resulting in 1500 and 2500 frames, respectively. Molecular Mechanics Poisson–Boltzmann Surface Area (MM/PBSA) binding free energy calculations were performed using the g_mmpbsa tool.^{49,50} The protocol closely followed the guidelines of the g_mmpbsa tutorials (<https://rashmikumari.github>).

io/g_mmpbsa/Tutorial.html) with the temperature set to 310 K. This analysis assessed the relative affinities of PPAR γ receptor residues for the ligands.

3. Results and Discussion

3.1. Stability of the systems and global structural analysis

The RMSD (Root Mean Square Deviation) (Figure 1) and RMSF (Root Mean Square Fluctuation) (Figure 2) analysis of the protein backbone and alpha-carbon did not reveal significant differences in global structural variations among the PPAR γ apo-form and PPAR γ -ligand complexes. Throughout the simulation period, all the systems remained stable. Additionally, the analysis of the average gyration radius of the alpha carbons of the protein indicated subtle variations in PPAR γ compactness during the simulations, consistent with overall protein stability observed in the RMSD results (Figures S1, Table S2; Supplementary Material).

Higher local flexibility was observed in less-ordered structures such as the Ω -loop (from I262 to E276), which is consistent with the more dynamic nature of this region.⁵¹⁻⁵³ Other PPAR γ secondary structures that showed greater relevance in this work were helices H2a (from K230 to L237), H2b (M252 to K261), H3 (V277 to K301), H4-H5 (from L311 to S332), H6-H7 (from K358 to A376), H10-H11 (from L431 to T459), H12 (from P467 to Y473), and the β -sheet region (from M334 to T349). Snapshots taken at both the initial and final stages of each simulation

are available in the Supplementary Material, Figure S2. The subtle differences among the system simulations may be attributed to specific interactions between the ligands and protein residues, influencing their ability to restrict or allow conformational changes. Therefore, a more detailed analysis of the interactions between the ligands and PPAR γ amino acids was conducted to elucidate potential sites for ligand recognition and affinity.

3.2. Hydrogen bonds

The results obtained from VMD and AMBER were highly comparable. The major residues engaged in hydrogen bonding with one or more specific ligands were K263 (Ω -loop), R280 (H3), R288 (H3), Y327 (H4-H5), and K367 (H6-H7), predominantly through their side chains, E343 (β -sheets) through its backbone, and K265 (Ω -loop), H266 (Ω -loop) and S342 (β -sheets) through their side chains and their backbones. Notably, the residues acted as bond donors in all the interactions. The frequency values obtained from VMD calculations are shown in Table 1. For comparison with values from AMBER, see Table S3 in the Supplementary Material.

3.3. Radial distribution function

Radial distribution function (RDF) analysis was employed to determine the functional groups of the ligands that were most likely to be involved in the observed hydrogen bonds. The calculations evaluated the average distance between the residues identified in the hydrogen

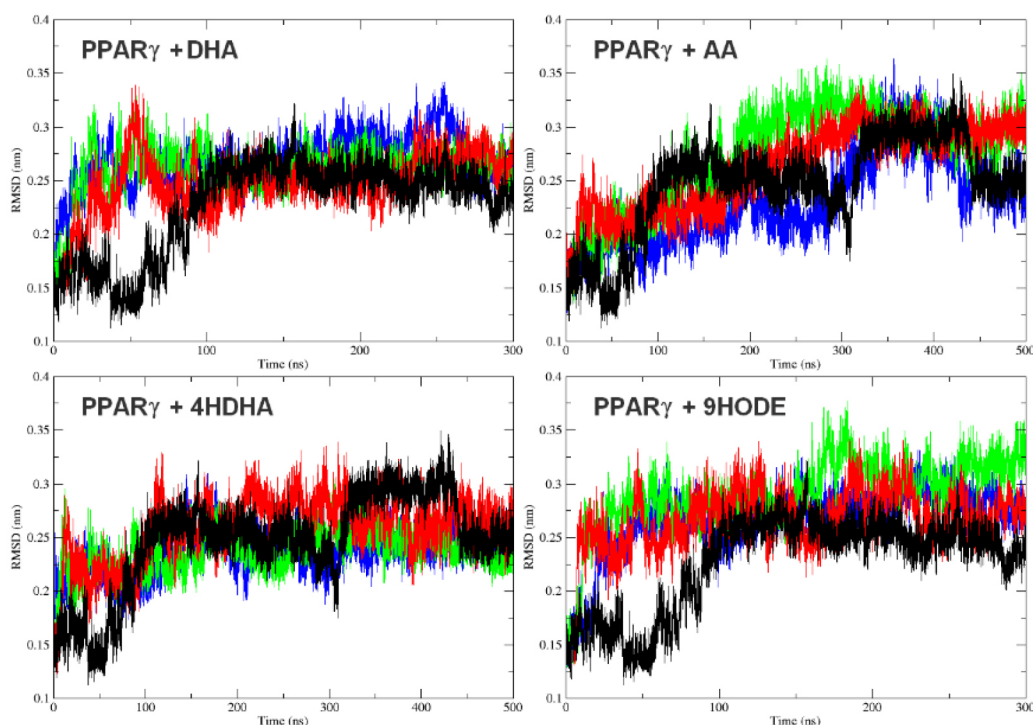


Figure 1. Root mean square deviation (RMSD) analysis of apo-PPAR γ and PPAR γ -ligand complexes. Simulations are depicted in different colors: the apo-system (black) and the complexed systems replicas r1 (red), r2 (green) and r3 (blue)

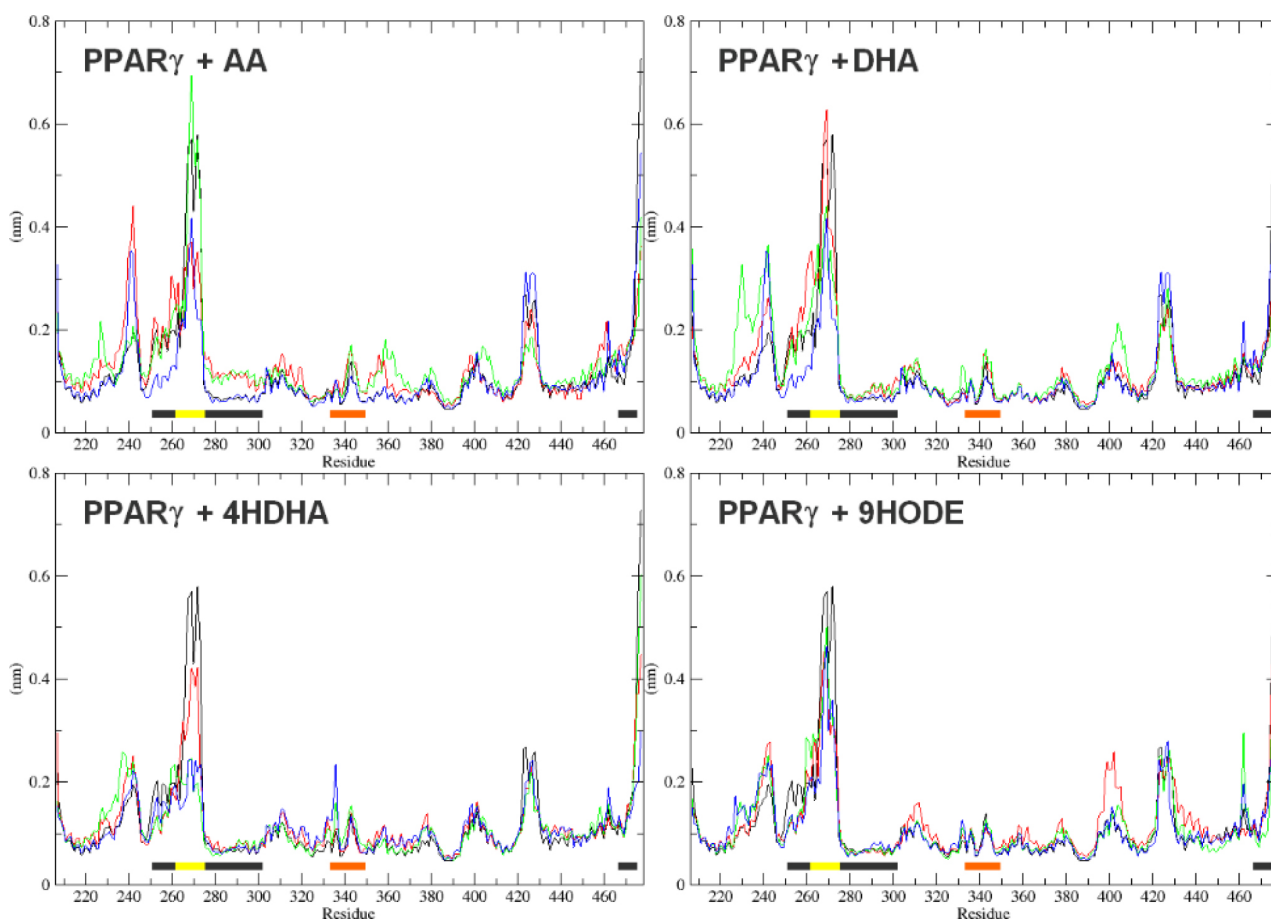


Figure 2. Root mean square fluctuation (RMSF) analysis of apo-PPAR γ and PPAR γ -ligand complexes. Simulations are depicted in different colors: the apo-system (black) and the complexed systems replicas r1 (red), r2 (green) and r3 (blue). The residue sequences of major regions in the protein are indicated by bars: from left to right, α -helices H2b, H3 and H12 (black bars), Ω -loop (yellow bar), β -sheet region (orange bar)

bonds, the carboxylic carbons (C1 in all four ligands), and the carbon atoms to which the hydroxyl radicals were attached (C4 and C9 in 4HDHA and 9HODE, respectively).

The results for the AA and DHA ligands indicate that the residues exhibiting the highest hydrogen bond frequencies were also those with the shortest average distances to the carboxylate groups of the ligands throughout the simulation period (Figure 3).

For the hydroxylated lipids 4HDHA and 9HODE, the distances from their carboxylate and hydroxyl groups to the residues were compared (Figure 4). For the 4HDHA ligand, R280, H266, S342, and R288 were closer to the carboxylate moiety but also showed considerable proximity to the hydroxyl group, whereas K265 (r2) was nearly equidistant from both groups throughout the simulation. For 9HODE, residues R280, K265, and K263 were closer to the carboxylate group. This trend was also evident for S342 during r1; however, a distinct pattern emerged for r2, in which S342 showed a notably more substantial interaction peak with the hydroxyl radical than with the carboxylate group. Although its interaction with carboxylate was less prominent, it was slightly more frequent at shorter distances than its interaction with the hydroxyl groups. In r3, S342 demonstrated

nearly equivalent distances from both functional groups, indicating a balanced interaction profile.

Different positions of the organic groups in the hydrocarbon chains of modified fatty acid agonists such as 9HODE and 4HDHA may play a role in determining the specificity of the ligand that binds to PPAR γ . The RDF results indicated that K265, H266, R280, R288, and S342 were likely to form hydrogen bonds with both the carboxylate and hydroxyl groups of the 4HDHA and 9HODE ligands.

3.4. MM/PBSA and Per Residue Protein-Ligand Interactions

The interactions between the residues and ligands reveal how the chemical structures of the ligands affect their binding to PPAR γ . RDF analysis identified the key residues engaged in hydrogen bonding, whereas MM/PBSA calculations elucidated the energetic aspects, highlighting the significance of the positively charged residues.

MM/PBSA calculations revealed that positively charged residues exhibited the most negative total binding energies (Table S4, Supplementary Material), which could be attributed to their stronger electrostatic interactions with the anionic polar heads of lipids and/or ion-dipole interactions

Table 1. Hydrogen bond frequencies in the protein-ligand complexes simulations, according to VMD Timeline Hydrogen Bonds calculations

Ligand	Simulation Replica	Residues	Hydrogen Bonds Frequency
AA ^a	r1	K265	0.23
		R288	0.15
		S342	0.49
		E343	0.11
	r2	R288	0.48
	S342	0.34	
DHA ^b	r3	R288	0.38
		S342	0.77
	r1	Y327	0.86
		K367	0.68
	r2	Y327	0.77
	K367	0.73	
4HDHA ^c	r1	H266	0.43
		R280	0.93
	r2	K265	0.10
		H266	0.48
	R280	0.91	
	r3	K265	0.56
S342		0.82	
E343		0.11	
9HODE ^d	r1	K265	0.32
		R280	0.29
		S342	0.60
	r2	K263	0.21
	R280	0.62	
	r3	R280	0.83
S342	0.14		

^aArachidonic acid; ^bdocosahexaenoic acid; ^c4-hydroxydocosahexaenoic acid; ^d9-hydroxyoctadecadienoic acid.

with hydroxyl radicals. The residues that displayed the more favorable binding energy (≤ -4.5 kcal.mol⁻¹): R288 (H3); K263 (Ω -loop) and K265 (Ω -loop); K232 (H2), K261 (H2b) and R280 (H3); K275 (Ω -loop) and K457 (H10-H11); and K367 (H6-H7).

Although the electrically neutral residues did not exhibit energy values as favorable as those of the positive residues, many of them participated in extensive networks of hydrophobic and polar interactions with various natural and synthetic PPAR γ agonists, playing crucial roles in the affinity of fatty acids, especially those with long hydrocarbon tails that might extend deep into the receptor pocket.⁵⁴⁻⁵⁸ F264 and H266 from the Ω -loop, I281 and C285 from H3, Y327 and L330 from H4-H5, I341, and M348 from the β -sheets region, and M364 from H6-H7 showed the lowest total binding energy values (≤ -1 kcal.mol⁻¹) among the noncharged residues in at least one simulation replica (Table S5, Supplementary material).

3.5. Comparative analysis of hydrogen bonding, RDF, and per residue MM/PBSA

Typical PPAR γ full agonists, such as TZDs, stabilize a critical protein surface for coregulator recognition,

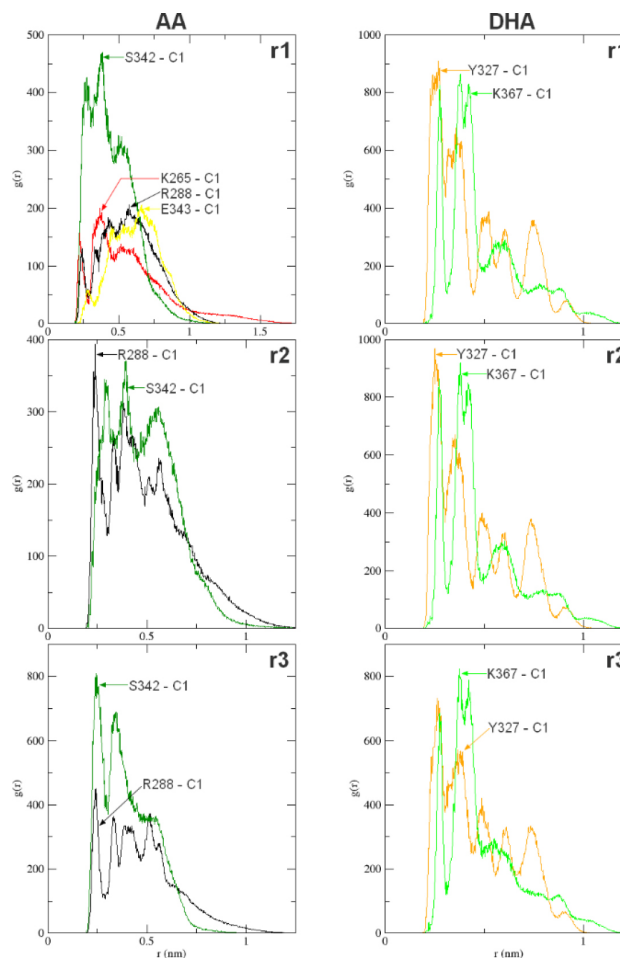


Figure 3. Average distances between carboxylate carbons (C1) in AA and DHA ligands and hydrogen-bonded residues were determined using RDF calculations. The x-axis represents the ligand's atom-to-residue distance (r), while the y-axis represents the $g(r)$ values, indicating the distribution and frequency of interactions during the simulation

activation function 2 (AF-2), interacting with H12 via direct or water-mediated contact with the Y473 residue.⁵⁸⁻⁶¹ Conversely, many studies have shown that partial agonists from different chemical classes do not interact directly with H12 but differentially stabilize other regions of the binding pocket of PPAR γ , as the H3 and the β -sheets.⁶² Situated at the entrance to the binding site, the highly flexible Ω -loop also plays a pivotal role in PPAR γ activation, by allowing ligands, particularly partial agonists, to enter without significantly changing the overall structure of the LBD.⁵²

In this study, most of the residues presenting stronger and more frequent interactions with the ligands belonged to these three regions (K263, F264, K265, H266, and K275 from the Ω -loop; R280, I281, C285, and R288 from H3; and I341, S342, E343, and M348 from the β -sheets). From hydrogen bonding and MM/PBSA analysis, together with the polar or nonpolar character of these residues, we can conclude that the Ω -loop interacted with the ligands primarily via electrostatic contacts and hydrogen bonds, and the β -sheet region primarily via hydrogen bonds and

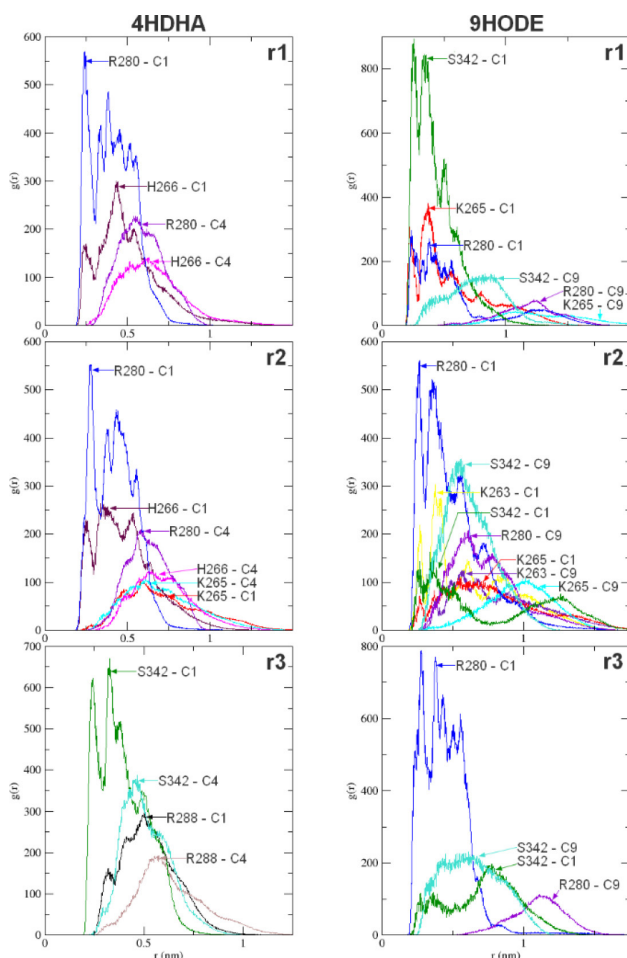


Figure 4. Average distances between the hydrogen bonded residues and carboxylate carbons (C1) and hydroxyl-attached carbons (C4 for 4HDHA and C9 for 9HODE) in the ligands

hydrophobic interactions, while H3 showed these three interaction types nearly equivalently.

The findings strongly corroborate with previous studies demonstrating that PPAR γ partial agonists, located between H3 and the β -sheets region, usually form a combination of hydrogen bonds with the backbone amide of S342 (β -sheet), electrostatic interactions with R288 (H3), and extensive van der Waals interactions with I341 (β -sheet) and C285 (H3).^{16,57} Residues from the H2, H2b, H4-H5, H6-H7, and H10-H11 regions, although fewer in number, also played crucial roles in interactions with lipids. Figure 5 shows the major apolar, polar, and charged residues involved in the most favorable contacts with the respective ligands within the PPAR γ binding site, according to MM/PBSA and hydrogen bonding analyses.

The R288 residue stood out prominently, exhibiting the lowest total binding energy across all three simulation replicates for AA and DHA and two of the three replicates for both 4HDHA (r2 and r3) and 9HODE (r1 and r3) (Table S4, Supplementary Material). This finding is consistent with that of a previous study that employed a similar approach.⁶³ Its location in H3, at the center of the ligand-binding site,⁶² allows the residue to establish

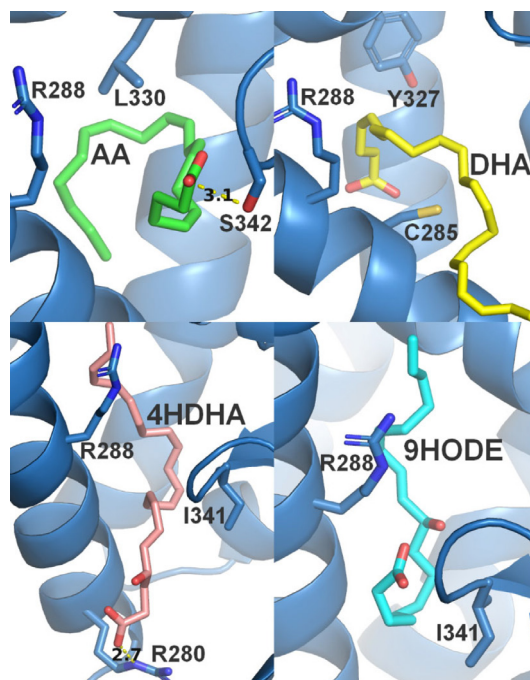


Figure 5. Ligands and interacting residues in PPAR γ binding site: MM/PBSA and hydrogen bonding analysis. S342 forms a hydrogen bond with AA carboxylate, while R280 interacts with 4HDHA carboxylate via a salt bridge (both interactions are represented by yellow dashed lines)

both electrostatic and extensive hydrophobic interactions with the ligands, facilitated by its long and flexible side chains.^{13,56,57,64-66}

Since R288 did not engage in any hydrogen bonds with 4HDHA and 9HODE within the 3.5 Å cut-off, a new RDF analysis was employed to further elucidate the relationship between the oxygenated groups of 4HDHA and 9HODE and R288 (Figure 6). In simulations r1 and r2 with 4HDHA, the residue remained closer to the hydroxyl group than to the carboxylate group, albeit with subtle interaction patterns. In r3, where R288 exhibited the lowest binding energy in our study ($-8.3 \text{ kcal}\cdot\text{mol}^{-1}$), shorter distances were observed to the carboxylate, yet prominent contacts were also established with the hydroxyl, indicating favorable interactions with both groups. For 9HODE, in r2, and especially in r3, R288 established significantly greater contact with the hydroxyl group than with the carboxylate group, whereas, in r1, the residue remained slightly closer to the carboxylate group, albeit with prominent peaks in both groups.

The side chain mobility of R288 is crucial for the adaptation of PPAR γ to different ligands.^{15,52} Furthermore, studies involving mutant receptors, where R288 is replaced by histidine (R288H), commonly found in colon cancers, demonstrated reduced affinity of PPAR γ for various fatty acid-derived agonists and increased movement of H3, both contributing to reduced receptor activity.^{17,31,67}

Other positively charged residues, notably R280 and K367, and, to a lesser extent, K265, frequently showed highly negative vacuum potential energies, indicating their

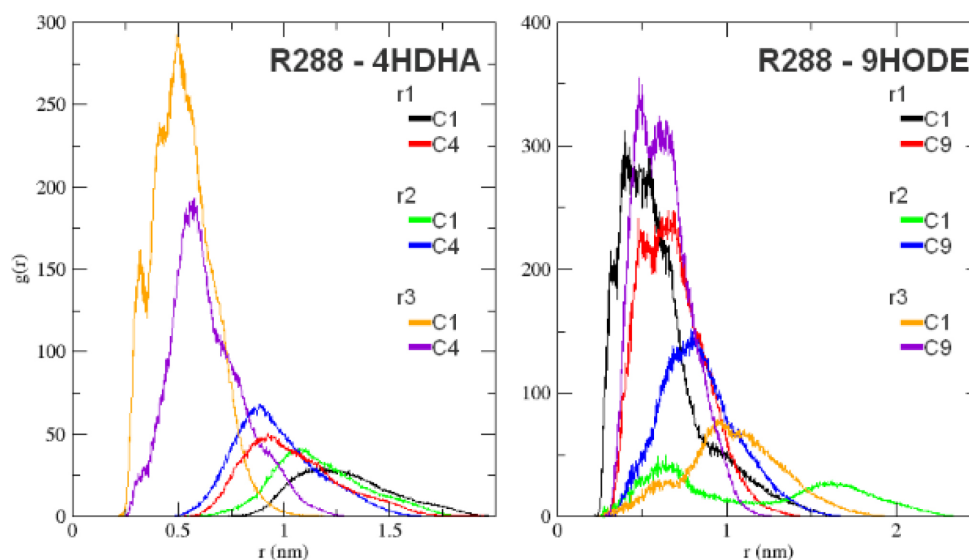


Figure 6. Proximity of the R288 residue to polar groups carboxylate and hydroxyl in 4HDHA and 9HODE ligands, according to RDF calculations

propensity to form hydrogen bonds. However, their total binding energies were less favorable than those observed for R288 (Table S6, Supplementary Material). This discrepancy in behavior among these positive residues can be attributed to the higher polar solvation energies typically exhibited by R280, K367, and K265.

Previous studies have shown that R280 plays a fundamental role in PPAR γ binding to many agonists via hydrogen bonds and electrostatic and hydrophobic interactions.^{65,68,69} The highly favorable contacts of arginine residues with anionic agonists may be better understood through quantum mechanical calculations, considering the resonance caused by electronic delocalization in the positively charged guanidinium moiety and the carboxylate groups of the ligands. Lysine residues, namely K263, K265, and K367, are also well-documented as pivotal participants in polar and electrostatic interactions with PPAR γ ligands.^{62,65,69,70} K263 and K265 might contribute significantly to the Ω -loop and H2b stabilization.^{58,64,65,71} In our simulations, K367 and Y327 were engaged in persistent hydrogen bonding with DHA. Previous structural and molecular docking studies have demonstrated the critical role of K367 in synergism with Y327 in establishing essential hydrogen bonds with hydroxy- and oxo-fatty acids derived from DHA and EPA and that the specific positioning of these amino acid side chains significantly affects ligand specificity to the receptor.^{16,17,31}

C285 stood out as the neutral residue with binding energy ≤ -1.3 kcal.mol⁻¹ in all the simulations with the four ligands (Table S5, Supplementary material). Several structural studies have demonstrated that the covalent coupling of C285 with modified lipids such as oxo- and nitro-fatty acids is crucial for PPAR γ activation.^{15,17,72} Noncovalent interactions with these lipids are associated with different conformations of the Ω -loop and distinct degrees of receptor activity (strong or weak). Moreover,

the amino acid side chains around C285 rearranged to the active conformation after covalent linkage.^{64,73,74} This residue can also form a narrow hydrophobic tunnel for ligand binding, along with I326 and L330.^{75,76} A similar behavior might be the case here, since L330 and, to a lesser extent I341, also stood out with relatively favorable energies in all simulations, and I281 in all DHA, 4HDHA, and 9HODE simulations, indicating a likely synergism between C285 and these hydrophobic residues.

Residues F264, H266, Y327, M348, and M364 often exhibit ligand-specific and subtle energetic contributions. In the r1 and r2 simulations with DHA, Y327 displayed the lowest binding energy values (approx. -1.0 kcal.mol⁻¹), which is consistent with the hydrogen bond frequencies in these replicas. Interestingly, these were the same replicates, in which DHA showed the most favorable interaction energy with C285. The side chain of Y327 catalyzes the formation of covalent bonds between C285 and oxo-fatty acids.¹⁵ In addition to the previously discussed role of Y327 with K267, our findings may further elucidate the synergistic behavior between Y327 and C285, by which persistent hydrogen bonds between Y327 and the ligand may partially restrict the latter movement, favoring its interaction with C285.

Although S342 did not exhibit any significant interaction energy in the MM/PBSA calculations, it emerged as a crucial hydrogen bond donor for AA, 4HDHA, and 9HODE. Previous structural studies have underscored the role of the hydrogen bonding of S342 with oxidized fatty acids, such as 13HODE (a 9HODE regioisomer).^{13,57,64} Docking and MD studies further demonstrated the bonding interactions of S342, extending its involvement to nonoxidized fatty acids within the ligand-binding pocket and emphasizing its significance in stabilizing PPAR γ partial agonists.^{27,77}

Molecular Dynamics calculations are applied to the models of ML-PPAR γ complexes in biological fluids and have advanced, allowing for the exploration of properties

and characteristics that increasingly and closely resemble related experimental observations.^{11,78} However, one of the greatest challenges in obtaining structural information on the interaction of LMs with PPAR γ is the immense diversity and conformational freedom of ligands within the enormous binding site.^{16,52} Using a range of analytical methods, we detailed the specific interactions between PPAR γ residues. Our in-depth analysis of these interactions provided valuable insights into the molecular mechanisms underlying the pivotal connections between PPAR γ and these lipid mediators.

Collectively, these findings enhance the understanding of PPAR γ -ligand interactions, paving the way for future research endeavors and potential therapeutic developments targeting the essential residues for molecular recognition and affinity. As the intricate mechanisms governing these interactions are elucidated, the therapeutic potential of these insights may be harnessed more effectively.

4. Conclusions

In this study, molecular dynamics calculations were employed to evaluate the interactions of PPAR γ protein with four of its natural, endogenous partial agonists from the n-3 and n-6 fatty acid series: AA, DHA, 4HDHA, and 9HODE. This comprehensive analysis sheds light on the intricate interplay between the receptor and its ligands. Specific amino acid residues, primarily from the protein's H3, Ω -loop, and β -sheet regions, and to a lesser extent from the H2a, H2b, H4-H5, H6-H7, H10-H11, and H12 regions, were found to be crucial for ligand interactions. The analysis revealed variations in the number, strength, and preferences of hydrogen bonding between PPAR γ and the different ligands. Residues R280, Y327, S342, and K367 engage in high-frequency hydrogen bonding with particular ligands. The MM/PBSA approach highlighted positively charged residues, such as K263, K265, R280, and particularly R288, as most energetically favorable for ligand binding. Residues with more hydrophobic side chains, such as I281, L330, I341, and especially C285, also presented favorable energy values and played significant roles in the interactions with different ligands. RDF calculations showed that carboxylates in the anionic polar heads of lipids are most probably involved in more persistent and stronger contacts, particularly hydrogen bonds, with the highlighted residues. However, some residues, such as K265, and mainly R288 and S342, demonstrated a more balanced interaction profile between the carboxylate and hydroxyl groups during the simulations with the oxidized ligands.

The residues exhibiting the lowest binding energy and highest hydrogen bond frequencies in each complex were pivotal in the interaction between the PPAR γ receptor and its specific ligands. This underscores the importance of statistical analysis of various molecular dynamics studies with diverse lipid mediators to elucidate the agonistic

mechanisms of this protein. The findings presented here may contribute to the development of new agonists with therapeutic potential for various health conditions, including metabolic disorders and inflammatory diseases related to the PPAR γ receptor. Consequently, targeting the key residues identified in this study may lead to the development of more specific therapeutic strategies with fewer adverse effects.

Supplementary Material

This work contains supplementary material available at: <https://rvq.s bq.org.br>

Acknowledgments

We extend our sincere appreciation to the Fundação de Amparo à Pesquisa do Estado de Minas Gerais (FAPEMIG), Conselho Nacional de Desenvolvimento Científico e Tecnológico (CNPq), and Fundação de Ensino e Pesquisa de Uberaba (FUNEPU). Special thanks go to Laboratório de Química Computacional Medicinal (LQCM)/ Instituto de Ciências Biológicas e Naturais (ICBN) at Universidade Federal do Triângulo Mineiro (UFTM) as well as to Laboratório Nacional de Computação Científica (LNCC) and Instituto Federal de Educação, Ciência e Tecnologia de Minas Gerais (IFMG).

Bibliographic References

1. Murakami, M.; Lipid Mediators in Life Science. *Experimental Animals* **2011**, *60*, 7. [[Crossref](#)] [[PubMed](#)]
2. Marion-Letellier, R.; Savoye, G.; Ghosh, S.; Fatty acids, eicosanoids and PPAR gamma. *European Journal of Pharmacology* **2016**, *785*, 44. [[Crossref](#)] [[PubMed](#)]
3. Berger, J.; Moller, D. E.; The mechanisms of action of PPARs. *Annual Review of Medicine* **2002**, *53*, 409. [[Crossref](#)] [[PubMed](#)]
4. Kliewer, S. A.; Lenhard, J. M.; Willson, T. M.; Patel, L.; Morris, D. C.; Lehmann, J. M.; A Prostaglandin J2 Metabolite Binds Peroxisome Proliferator-Activated Receptor γ and Promotes Adipocyte Differentiation. *Cell* **1995**, *83*, 813. [[Crossref](#)] [[PubMed](#)]
5. Fujita, T.; Sugiyama, Y.; Taketomi, S.; Sohda, T.; Kawamatsu, Y.; Iwatsuka, H.; Suzuoki, Z.; Reduction of Insulin Resistance in Obese and/or Diabetic Animals by 5-[4-(1Methylcyclohexylmethoxy)benzyl]-thiazolidine-2,4-dione (ADD-3878, U-63,287, Ciglitazone), a New Antidiabetic Agent. *Diabetes* **1983**, *32*, 804. [[Crossref](#)]
6. Jones, D. C.; Manning, B. M.; Daynes, R. A.; A role for the peroxisome proliferator-activated receptor α in T-cell physiology and ageing immunobiology. *Proceedings of the Nutrition Society* **2002**, *61*, 363. [[Crossref](#)] [[PubMed](#)]
7. Glass, C. K.; Saijo, K.; Nuclear receptor transrepression

- pathways that regulate inflammation in macrophages and T cells. *Nature Reviews Immunology* **2010**, *10*, 365. [[Crossref](#)] [[PubMed](#)]
8. Wahli, W.; Michalik, L.; PPARs at the crossroads of lipid signaling and inflammation. *Trends in Endocrinology and Metabolism* **2012**, *23*, 351. [[Crossref](#)] [[PubMed](#)]
 9. Sheng, W.; Wang, Q.; Qin, H.; Cao, S.; Wei, Y.; Weng, J.; Yu, F.; Zeng, H.; Osteoarthritis: Role of Peroxisome Proliferator-Activated Receptors. *International Journal of Molecular Sciences* **2023**, *24*, 1. [[Crossref](#)] [[PubMed](#)]
 10. Marciano, D. P.; Kuruvilla, D. S.; Boregowda, S. V.; Asteian, A.; Hughes, T. S.; Garcia-Ordenez, R.; Corzo, C. A.; Khan, T. M.; Novick, S. J.; Park, H.; Kojetin, D. J.; Phinney, D. G.; Bruning, J. B.; Kamenecka, T. M.; Griffin, P. R.; Pharmacological repression of PPAR γ promotes osteogenesis. *Nature Communications* **2015**, *6*, 1. [[Crossref](#)] [[PubMed](#)]
 11. Harmon, G. S.; Lam, M. T.; Glass, C. K.; PPARs and lipid ligands in inflammation and metabolism. *Chemical Reviews* **2011**, *111*, 6321. [[Crossref](#)] [[PubMed](#)]
 12. Brust, R.; Lin, H.; Fuhrmann, J.; Asteian, A.; Kamenecka, T. M.; Kojetin, D. J.; Modification of the Orthosteric PPAR γ Covalent Antagonist Scaffold Yields an Improved Dual-Site Allosteric Inhibitor. *ACS Chemical Biology* **2017**, *12*, 969. [[Crossref](#)] [[PubMed](#)]
 13. Montanari, R.; Saccoccia, F.; Scotti, E.; Crestani, M.; Godio, C.; Gilardi, F.; Loiodice, F.; Fracchiolla, G.; Laghezza, A.; Tortorella, P.; Lavecchia, A.; Novellino, E.; Mazza, F.; Aschi, M.; Pochetti, G.; Crystal structure of the peroxisome proliferator-activated receptor γ (PPAR γ) ligand binding domain complexed with a novel partial agonist: A new region of the hydrophobic pocket could be exploited for drug design. *Journal of Medicinal Chemistry* **2008**, *51*, 7768. [[Crossref](#)] [[PubMed](#)]
 14. Ayza, M. A.; Zewdie, K. A.; Tesfaye, B. A.; Tesfamariam, S.; Gebrekirstos, Berhe, D. F.; Anti-diabetic effect of telmisartan through its partial ppar γ -agonistic activity. *Diabetes, Metabolic Syndrome and Obesity* **2020**, *13*, 3627. [[Crossref](#)] [[PubMed](#)]
 15. Itoh, T.; Fairall, L.; Amin, K.; Inaba, Y.; Szanto, A.; Balint, B. L.; Nagy, L.; Yamamoto, K.; Schwabe, J. W. R.; Structural basis for the activation of PPAR γ by oxidized fatty acids. *Nature Structural and Molecular Biology* **2008**, *15*, 924. [[Crossref](#)] [[PubMed](#)]
 16. Narala, V. R.; Subramani, P. A.; Narasimha, V. R.; Shaik, F. B.; Panati, K.; The role of nitrated fatty acids and peroxisome proliferator-activated receptor gamma in modulating inflammation. *International Immunopharmacology* **2014**, *23*, 283. [[Crossref](#)] [[PubMed](#)]
 17. Egawa, D.; Itoh, T.; Yamamoto, K.; Characterization of covalent bond formation between PPAR γ and Oxo-fatty acids. *Bioconjugate Chemistry* **2015**, *26*, 690. [[Crossref](#)] [[PubMed](#)]
 18. Toborek, M.; Lee, Y. W.; Garrido, R.; Kaiser, S.; Hennig, B.; Unsaturated fatty acids selectively induce an inflammatory environment in human endothelial cells. *The American Journal of Clinical Nutrition* **2002**, *75*, 119. [[Crossref](#)] [[PubMed](#)]
 19. James, M. J.; Cleland, L. G.; Dietary n-3 Fatty Acids and Therapy for Rheumatoid Arthritis. *Seminars in Arthritis and Rheumatism* **1997**, *27*, 85. [[Crossref](#)] [[PubMed](#)]
 20. Kremer, J. M.; n-3 Fatty acid supplements in rheumatoid arthritis. *The American Journal of Clinical Nutrition* **2000**, *71*, 349S. [[Crossref](#)] [[PubMed](#)]
 21. Hu, F. B.; Manson, J. A. E.; Willett, W. C.; Types of Dietary Fat and Risk of Coronary Heart Disease: A Critical Review. *Journal of the American College of Nutrition* **2001**, *20*, 5. [[Crossref](#)] [[PubMed](#)]
 22. Dalle, C.; Tournayre, J.; Mainka, M.; Basiak-Rasała, A.; Pétéra, M.; Lefèvre-Arbogast, S.; Dalloux-Chioccioli, J.; Deschasaux-Tanguy, M.; Lécuyer, L.; Kesse-Guyot, E.; Fezeu, L. K.; Hercberg, S.; Galan, P.; Samieri, C.; Zatońska, K.; Calder, P. C.; Hjorth, M. F.; Astrup, A.; Mazur, A.; Bertrand-Michel, J.; Schebb, N. H.; Szuba, A.; Touvier, M.; Newman, J. W.; Gladine, C.; The Plasma Oxylinin Signature Provides a Deep Phenotyping of Metabolic Syndrome Complementary to the Clinical Criteria. *International Journal of Molecular Sciences* **2022**, *23*, 11688. [[Crossref](#)] [[PubMed](#)]
 23. Fratev, F.; Steinbrecher, T.; Jónsdóttir, S. Ó.; Prediction of Accurate Binding Modes Using Combination of Classical and Accelerated Molecular Dynamics and Free-Energy Perturbation Calculations: An Application to Toxicity Studies. *ACS Omega* **2018**, *3*, 4357. [[Crossref](#)] [[PubMed](#)]
 24. Ju, Z.; Su, M.; Hong, J.; Ullah, S.; Kim, E. La; Zhao, C. H.; Moon, H. R.; Kim, S.; Jung, J. H.; Design of PPAR- γ agonist based on algal metabolites and the endogenous ligand 15-deoxy- Δ 12, 14-prostaglandin J2. *European Journal of Medicinal Chemistry* **2018**, *157*, 1192. [[Crossref](#)] [[PubMed](#)]
 25. Lewis, S. N.; Bassaganya-Riera, J.; Bevan, D. R.; Virtual Screening as a Technique for PPAR Modulator Discovery. *PPAR Research* **2010**, *2010*, 1. [[Crossref](#)] [[PubMed](#)]
 26. Azam, M. N. K.; Biswas, P.; Tareq, M. M. I.; Hossain, M. R.; Bibi, S.; Hoque, M. A.; Khandker, A.; Alam, M. A.; Zilani, M. N. H.; Rahman, M. S.; Albekairi, N. A.; Alshammari, A.; Hasan, M. N.; Identification of antidiabetic inhibitors from *Allophylus villosus* and *Mycetia sinensis* by targeting α -glucosidase and PPAR- γ : In-vitro, in-vivo, and computational evidence. *Saudi Pharmaceutical Journal* **2024**, *32*, 2. [[Crossref](#)] [[PubMed](#)]
 27. Musfiroh, I.; Megawati, G.; Herawati, D. M. D.; Ifaya, M.; Stability of omega-3 compounds complex with ppar- γ receptor as an anti-obesity using molecular dynamic simulation. *International Journal of Applied Pharmaceutics* **2022**, *14*, 45. [[Crossref](#)]
 28. Shiraki, T.; Kodama, T. S.; Jingami, H.; Kamiya, N.; Rational discovery of a novel interface for a coactivator in the peroxisome proliferator-activated receptor γ : Theoretical implications of impairment in type diabetes mellitus. *Proteins: Structure, Function and Genetics* **2005**, *58*, 418. [[Crossref](#)] [[PubMed](#)]
 29. Zhang, T.; Chen, X.; Ju, X.; Yuan, J.; Zhou, J.; Zhang, Z.; Ju, G.; Xu, D.; PPARG is a potential target of Tanshinone IIA in prostate cancer treatment: a combination study of molecular docking and dynamic simulation based on transcriptomic bioinformatics. *European Journal of Medical Research* **2023**, *28*, 1. [[Crossref](#)] [[PubMed](#)]
 30. Bull, A. W.; Steffensen, K. R.; Leers, J.; Rafter, J. J.; Activation of PPAR γ in colon tumor cell lines by oxidized metabolites of linoleic acid, endogenous ligands for PPAR γ . *Carcinogenesis* **2003**, *24*, 1717. [[Crossref](#)] [[PubMed](#)]

31. Li, Y.; Zhang, J.; Schopfer, F. J.; Martynowski, D.; Garcia-Barrio, M. T.; Kovach, A.; Suino-Powell, K.; Baker, P. R. S.; Freeman, B. A.; Chen, Y. E.; Xu, H. E.; Molecular recognition of nitrated fatty acids by PPAR γ . *Nature Structural and Molecular Biology* **2008**, *15*, 865. [[Crossref](#)] [[PubMed](#)]
32. Sapieha, P.; Stahl, A.; Chen, J.; Seaward, M. R.; Willett, K. L.; Krah, N. M.; Dennison, R. J.; Connor, K. M.; Christopher, †; Aderman, M.; Liclican, E.; Carughi, A.; Perelman, D.; Kanaoka, Y.; Sangiovanni, J. P.; Gronert, K.; Smith, L. E. H.; 5-Lipoxygenase Metabolite 4-HDHA Is a Mediator of the Antiangiogenic Effect of ω -3 Polyunsaturated Fatty Acids. *Science Translational Medicine* **2011**, *3*, 1. [[Crossref](#)] [[PubMed](#)]
33. Eswar, N.; Webb, B.; Marti-Renom, M. A.; Madhusudhan, M. S.; Eramian, D.; Shen, M.; Pieper, U.; Sali, A.; Comparative Protein Structure Modeling Using MODELLER. *Current Protocols in Protein Science* **2007**, *50*, 1. [[Crossref](#)] [[PubMed](#)]
34. Berman, H. M.; Westbrook, J.; Feng, Z.; Gilliland, G.; Bhat, T. N.; Weissig, H.; Shindyalov, I. N.; Bourne, P. E.; The Protein Data Bank. *Nucleic Acids Research* **2000**, *28*, 235. [[Crossref](#)] [[PubMed](#)]
35. Colovos, C.; Yeates, T. O.; Verification of protein structures: Patterns of nonbonded atomic interaction. *Protein Science* **1993**, *2*, 1511. [[Crossref](#)] [[PubMed](#)]
36. Schrödinger Release 2024-3: Maestro, Schrödinger, LLC, New York, NY, 2024. [[Link](#)]
37. De Magalhães, C. S.; Almeida, D. M.; Barbosa, H. J. C.; Dardenne, L. E.; A dynamic niching genetic algorithm strategy for docking highly flexible ligands. *Information Sciences* **2014**, *289*, 206. [[Crossref](#)]
38. Guedes, I. A.; Barreto, A. M. S.; Marinho, D.; Krempser, E.; Kuenemann, M. A.; Sperandio, O.; Dardenne, L. E.; Miteva, M. A.; New machine learning and physics-based scoring functions for drug discovery. *Scientific Reports* **2021**, *11*, 1. [[Crossref](#)] [[PubMed](#)]
39. Jo, S.; Kim, T.; Iyer, V. G.; Im, W.; CHARMM-GUI: A web-based graphical user interface for CHARMM. *Journal of Computational Chemistry* **2008**, *29*, 1859. [[Crossref](#)] [[PubMed](#)]
40. Vanommeslaeghe, K.; Raman, E. P.; MacKerell, A. D.; Automation of the CHARMM General Force Field (CGenFF) II: Assignment of Bonded Parameters and Partial Atomic Charges. *Journal of Chemical Information and Modeling* **2012**, *52*, 3155. [[Crossref](#)] [[PubMed](#)]
41. Yu, W.; He, X.; Vanommeslaeghe, K.; MacKerell, A. D.; Extension of the CHARMM general force field to sulfonyl-containing compounds and its utility in biomolecular simulations. *Journal of Computational Chemistry* **2012**, *33*, 2451. [[Crossref](#)] [[PubMed](#)]
42. Vanommeslaeghe, K.; Hatcher, E.; Acharya, C.; Kundu, S.; Zhong, S.; Shim, J.; Darian, E.; Guvench, O.; Lopes, P.; Vorobyov, I.; Mackerell, A. D.; CHARMM general force field: A force field for drug-like molecules compatible with the CHARMM all-atom additive biological force fields. *Journal of Computational Chemistry* **2010**, *31*, 671. [[Crossref](#)] [[PubMed](#)]
43. Evans, D. J.; Holian, B. L.; The Nose-Hoover thermostat. *The Journal of Chemical Physics* **1985**, *83*, 4069. [[Crossref](#)]
44. Parrinello, M.; Rahman, A.; Polymorphic transitions in single crystals: A new molecular dynamics method. *Journal of Applied Physics* **1981**, *52*, 7182. [[Crossref](#)]
45. Kolafa, J.; Perram, J. W.; Cutoff Errors in the Ewald Summation Formulae for Point Charge Systems. *Molecular Simulation* **1992**, *9*, 351. [[Crossref](#)]
46. Berendsen, H. J. C.; Van Der Spoel, D.; Van Drunen, R.; GROMACS: A message-passing parallel molecular dynamics implementation. *Computer Physics Communications* **1995**, *91*, 43. [[Crossref](#)]
47. Humphrey, W.; Dalke, A.; Schulten, K.; VMD: Visual Molecular Dynamics. *Journal of Molecular Graphics* **1996**, *14*, 33. [[Crossref](#)]
48. Cornell, W. D.; Cieplak, P.; Bayly, C. I.; Gould, I. R.; Merz, K. M.; Ferguson Jr, D. M.; Spellmeyer, D. C.; Fox, T.; Caldwell, J. W.; Kollman, P. A.; A Second Generation Force Field for the Simulation of Proteins, Nucleic Acids, and Organic Molecules. *Journal of the American Chemical Society* **1995**, *117*, 5179. [[Crossref](#)]
49. Kumari, R.; Kumar, R.; Lynn, A.; G-mmpbsa -A GROMACS tool for high-throughput MM-PBSA calculations. *Journal of Chemical Information and Modeling* **2014**, *54*, 1951. [[Crossref](#)] [[PubMed](#)]
50. Baker, N. A.; Sept, D.; Joseph, S.; Holst, M. J.; Andrew McCammon, J.; Electrostatics of nanosystems: Application to microtubules and the ribosome. *Proceedings of the National Academy of Sciences* **2001**, *98*, 10037. [[Crossref](#)] [[PubMed](#)]
51. Xu, H. E.; Lambert, M. H.; Montana, V. G.; Parks, D. J.; Blanchard, S. G.; Brown, P. J.; Sternbach, D. D.; Rgen, J.; Lehmann, M.; Wisely, G. B.; Willson, T. M.; Kliewer, S. A.; Milburn, M. V.; Molecular Recognition of Fatty Acids by Peroxisome Proliferator-Activated Receptors. *Molecular Cell* **1999**, *3*, 397. [[Crossref](#)]
52. Zoete, V.; Grosdidier, A.; Michielin, O.; Peroxisome proliferator-activated receptor structures: Ligand specificity, molecular switch and interactions with regulators. *Biochimica et Biophysica Acta - Molecular and Cell Biology of Lipids* **2007**, *1771*, 915. [[Crossref](#)] [[PubMed](#)]
53. Ricci, C. G.; Silveira, R. L.; Rivalta, I.; Batista, V. S.; Skaf, M. S.; Allosteric Pathways in the PPAR γ -RXR α nuclear receptor complex. *Scientific Reports* **2016**, *6*, 1. [[Crossref](#)] [[PubMed](#)]
54. Mahindroo, N.; Peng, Y. H.; Lin, C. H.; Tan, U. K.; Prakash, E.; Lien, T. W.; Lu, I. L.; Lee, H. J.; Hsu, J. T. A.; Chen, X.; Liao, C. C.; Lyu, P. C.; Chao, Y. S.; Wu, S. Y.; Hsieh, H. P.; Structural basis for the structure-activity relationships of peroxisome proliferator-activated receptor agonists. *Journal of Medicinal Chemistry* **2006**, *49*, 6421. [[Crossref](#)] [[PubMed](#)]
55. Bruning, J. B.; Chalmers, M. J.; Prasad, S.; Busby, S. A.; Kamenecka, T. M.; He, Y.; Nettles, K. W.; Griffin, P. R.; Partial Agonists Activate PPAR γ Using a Helix 12 Independent Mechanism. *Structure* **2007**, *15*, 1258. [[Crossref](#)] [[PubMed](#)]
56. Van Marrewijk, L. M.; Polyak, S. W.; Hijnen, M.; Kuruvilla, D.; Chang, M. R.; Shin, Y.; Kamenecka, T. M.; Griffin, P. R.; Bruning, J. B.; SR2067 Reveals a Unique Kinetic and Structural Signature for PPAR γ Partial Agonism. *ACS Chemical Biology* **2016**, *11*, 273. [[Crossref](#)] [[PubMed](#)]

57. Capelli, D.; Cerchia, C.; Montanari, R.; Loiodice, F.; Tortorella, P.; Laghezza, A.; Cervoni, L.; Pochetti, G.; Lavecchia, A.; Structural basis for PPAR partial or full activation revealed by a novel ligand binding mode. *Scientific Reports* **2016**, *6*, 1. [[Crossref](#)] [[PubMed](#)]
58. Brust, R.; Shang, J.; Fuhrmann, J.; Mosure, S. A.; Bass, J.; Cano, A.; Heidari, Z.; Chrisman, I. M.; Nemetchek, M. D.; Blayo, A. L.; Griffin, P. R.; Kamenecka, T. M.; Hughes, T. S.; Kojetin, D. J.; A structural mechanism for directing corepressor-selective inverse agonism of PPAR γ . *Nature Communications* **2018**, *9*, 1. [[Crossref](#)] [[PubMed](#)]
59. Yu, C.; Chen, L.; Luo, H.; Chen, J.; Cheng, F.; Gui, C.; Zhang, R.; Shen, J.; Chen, K.; Jiang, H.; Shen, X.; Binding analyses between Human PPAR γ -LBD and ligands: Surface plasmon resonance biosensor assay correlating with circular dichroic spectroscopy determination and molecular docking. *European Journal of Biochemistry* **2004**, *271*, 386. [[Crossref](#)] [[PubMed](#)]
60. Malapaka, R. R. V.; Khoo, S. K.; Zhang, J.; Choi, J. H.; Zhou, X. E.; Xu, Y.; Gong, Y.; Li, J.; Yong, E. L.; Chalmers, M. J.; Chang, L.; Resau, J. H.; Griffin, P. R.; Chen, Y. E.; Xu, H. E.; Identification and mechanism of 10-carbon fatty acid as modulating ligand of peroxisome proliferator-activated receptors. *Journal of Biological Chemistry* **2012**, *287*, 183. [[Crossref](#)] [[PubMed](#)]
61. Xu, H. E.; Lambert, M. H.; Montana, V. G.; Plunket, K. D.; Moore, L. B.; Collins, J. L.; Oplinger, J. A.; Kliewer, S. A.; Gampe, R. T.; Mckee, D. D.; Moore, J. T.; Willson, T. M.; Rosenfeld, M. G.; Structural determinants of ligand binding selectivity between the peroxisome proliferator-activated receptors. *Proceedings of the National Academy of Sciences* **2001**, *98*, 13919. [[Crossref](#)] [[PubMed](#)]
62. Hanke, T.; Cheung, S. Y.; Kilu, W.; Heering, J.; Ni, X.; Planz, V.; Schierle, S.; Faudone, G.; Friedrich, M.; Wanior, M.; Werz, O.; Windbergs, M.; Proschak, E.; Schubert-Zsilavec, M.; Chaikwad, A.; Knapp, S.; Merk, D.; A selective modulator of peroxisome proliferator-activated receptor γ with an unprecedented binding mode. *Journal of Medicinal Chemistry* **2020**, *63*, 4555. [[Crossref](#)] [[PubMed](#)]
63. Álvarez-Almazán, S.; Bello, M.; Tamay-Cach, F.; Martínez-Archundia, M.; Alemán-González-Duhart, D.; Correa-Basurto, J.; Mendieta-Wejebe, J. E.; Study of new interactions of glitazone's stereoisomers and the endogenous ligand 15d-PGJ2 on six different PPAR gamma proteins. *Biochemical Pharmacology* **2017**, *142*, 168. [[Crossref](#)] [[PubMed](#)]
64. Waku, T.; Shiraki, T.; Oyama, T.; Morikawa, K.; Atomic structure of mutant PPAR γ LBD complexed with 15d-PGJ2: Novel modulation mechanism of PPAR γ /RXR α function by covalently bound ligands. *FEBS Letters* **2008**, *583*, 320. [[Crossref](#)] [[PubMed](#)]
65. Puhl, A. C.; Bernardes, A.; Silveira, R. L.; Yuan, J.; Campos, J. L. O.; Saidemberg, D. M.; Palma, M. S.; Cvaro, A.; Ayers, S. D.; Webb, P.; Reinach, P. S.; Skaf, M. S.; Polikarpov, I.; Mode of peroxisome proliferator-activated receptor γ activation by luteolin. *Molecular Pharmacology* **2012**, *81*, 788. [[Crossref](#)] [[PubMed](#)]
66. Puhl, A. C.; Milton, F. A.; Cvaro, A.; Sieglaff, D. H.; Campos, J. C. L.; Bernardes, A.; Filgueira, C. S.; Lindemann, J. L.; Deng, T.; Neves, F. A. R.; Polikarpov, I.; Webb, P.; Mechanisms of peroxisome proliferator activated receptor γ regulation by non-steroidal anti-inflammatory drugs. *Nuclear Receptor Signaling* **2015**, *13*, 1. [[Crossref](#)] [[PubMed](#)]
67. Egawa, D.; Ogiso, T.; Nishikata, K.; Yamamoto, K.; Itoh, T.; Structural Insights into the Loss-of-Function R288H Mutant of Human PPAR γ . *Biological and Pharmaceutical Bulletin* **2021**, *44*, 1196. [[Crossref](#)] [[PubMed](#)]
68. Jang, J. Y.; Bae, H.; Lee, Y. J.; Choi, Y. Il; Kim, H. J.; Park, S. B.; Suh, S. W.; Kim, S. W.; Han, B. W.; Structural Basis for the Enhanced Anti-Diabetic Efficacy of Lobeglitazone on PPAR γ . *Scientific Reports* **2018**, *8*, 1. [[Crossref](#)] [[PubMed](#)]
69. Lokhande, K. B.; Ballav, S.; Yadav, R. S.; Swamy, K. V.; Basu, S.; Probing intermolecular interactions and binding stability of kaempferol, quercetin and resveratrol derivatives with PPAR- γ : docking, molecular dynamics and MM/GBSA approach to reveal potent PPAR- γ agonist against cancer. *Journal of Biomolecular Structure and Dynamics* **2022**, *40*, 971. [[Crossref](#)] [[PubMed](#)]
70. Nolte, R. T.; Wisely, G. B.; Westin, S.; Cobb, J. E.; Lambert, M. H.; Kurokawa, R.; Rosenfeldk, M. G.; Willson, T. M.; Glass, C. K.; Milburn, M. V.; Ligand binding and co-activator assembly of the peroxisome proliferator-activated receptor gamma. *Nature* **1998**, *395*, 137. [[Crossref](#)]
71. Stalin, A.; Lin, D.; Josephine Princy, J.; Feng, Y.; Xiang, H.; Ignacimuthu, S.; Chen, Y.; Computational analysis of single nucleotide polymorphisms (SNPs) in PPAR gamma associated with obesity, diabetes and cancer. *Journal of Biomolecular Structure and Dynamics* **2022**, *40*, 1843. [[Crossref](#)] [[PubMed](#)]
72. Cipollina, C.; Salvatore, S. R.; Muldoon, M. F.; Freeman, B. A.; Schopfer, F. J.; Generation and Dietary Modulation of Anti-Inflammatory Electrophilic Omega-3 Fatty Acid Derivatives. *PLoS ONE* **2014**, *9*, 1. [[Crossref](#)] [[PubMed](#)]
73. Waku, T.; Shiraki, T.; Oyama, T.; Maebara, K.; Nakamori, R.; Morikawa, K.; The nuclear receptor PPAR γ individually responds to serotonin-and fatty acid-metabolites. *The European Molecular Biology Organization Journal* **2010**, *29*, 3395. [[Crossref](#)] [[PubMed](#)]
74. Waku, T.; Shiraki, T.; Oyama, T.; Fujimoto, Y.; Maebara, K.; Kamiya, N.; Jingami, H.; Morikawa, K.; Structural Insight into PPAR γ Activation Through Covalent Modification with Endogenous Fatty Acids. *Journal of Molecular Biology* **2009**, *385*, 188. [[Crossref](#)] [[PubMed](#)]
75. Yamamoto, K.; Itoh, T.; Abe, D.; Shimizu, M.; Kanda, T.; Koyama, T.; Nishikawa, M.; Tamai, T.; Ooizumi, H.; Yamada, S.; Identification of putative metabolites of docosahexaenoic acid as potent PPAR γ agonists and antidiabetic agents. *Bioorganic and Medicinal Chemistry Letters* **2005**, *15*, 517. [[Crossref](#)] [[PubMed](#)]
76. Useini, A.; Engelberger, F.; Künze, G.; Sträter, N.; Structural basis of the activation of PPAR γ by the plasticizer metabolites MEHP and MINCH. *Environment International* **2023**, *173*, 1. [[Crossref](#)] [[PubMed](#)]

77. Jian, Y.; He, Y.; Yang, J.; Han, W.; Zhai, X.; Zhao, Y.; Li, Y.; Molecular modeling study for the design of novel peroxisome proliferator-activated receptor gamma agonists using 3D-QSAR and molecular docking. *International Journal of Molecular Sciences* **2018**, *19*, 1. [[Crossref](#)] [[PubMed](#)]
78. Alexander, R. L.; Wright, M. W.; Gorczynski, M. J.; Smitherman, P. K.; Akiyama, T. E.; Wood, H. B.; Berger, J. P.; King, S. B.; Morrow, C. S.; Differential Potencies of Naturally Occurring Regioisomers of Nitrolinoleic Acid in PPAR γ Activation. *Biochemistry* **2008**, *48*, 492. [[Crossref](#)] [[PubMed](#)]